

Upslope Walking with Transfemoral Prosthesis Using Optimization Based Spline Generation

Victor Paredes¹, Woolim Hong¹, Shawanee Patrick¹ and Pilwon Hur¹

Abstract—Powered transfemoral prostheses are robotic systems that aim to restore the mobility of transfemoral amputees by mimicking the functionalities of healthy human legs. The advantage of using a powered prosthetic device is the enhanced performance on various terrains. One of the most frequent terrain found during daily locomotion (other than flat ground) is the surface with slope. In this work, we introduce a framework to generate upslope walking gaits automatically utilizing an online algorithmic formulation. This approach is inspired from analyzing human gait characteristics during upslope walking. In particular, it is found that the ankle and knee trajectories of upslope walking share a similar pattern with flat ground walking during the middle section (from 20% to 80%) of one step. This observation motivates us to propose an approach of blending the first portion of nominal flat ground gaits with a set of cubic splines to achieve upslope gaits. Importantly, parameters of these cubic splines are solved using an online optimization, which gives the users ability to traverse in different terrains without using any intention detection algorithm. For the last portion of a step, an impedance controller with low gains is considered upon the contact of prosthetic legs to the ground, which allows the users to step onto unknown terrains. The proposed framework is validated on a custom transfemoral prosthesis AMPRO II with showing automatic motion switches between flat ground and upslope walking.

I. INTRODUCTION

It is estimated that there are approximately 185,000 new amputation each year in the United States [1]. According to the National Center for Health Statistics [2], among the total 1.2 million people in the United States living with limb losses, 18.5% are transfemoral amputees. Amputation affects the mobility of impaired subjects and limits their activities of daily living. The use of prosthetic devices is aimed at restoring the walking capabilities of amputees by mimicking the behavior of a normal gait. In particular, there are certain requirements that must be met for prostheses. For instance, prostheses must support the human body weight, reduce the metabolic energy consumption and be able to take cues from the users. Based on whether a prosthesis can provide net power during walking or not, there are two main types of prostheses: i) energetic passive devices and ii) powered devices. Despite the apparent advantages of powered prostheses (being able to provide net power), most of the market is centered on passive devices. An important

drawback of passive devices is the lack of adaptability to different terrains, such as upslope and upstairs. Since most environments include both flat and sloped surfaces, user-oriented transfemoral prostheses should be able to produce walking gaits in those terrains flawlessly. However, most of the powered transfemoral prostheses have been focused only on flat ground walking [3], [4], [5]. With the purpose of exploring solutions for traversing sloped surfaces, we take our first steps to propose a framework for automatically generating upslope walking gaits with online optimization.

While powered flat ground prosthetic walking has been studied vigorously, only limited research for upslope walking can be found. Sup et al. [6] proposed a motion transition method with a transfemoral prosthesis that has demonstrated successful walkings for different terrains. This work proposed to tune impedance parameters for different phases and slope inclinations. Based on the estimated inclination angle, the impedance parameters with the best matching inclination angle in the database were chosen. However, because the dataset can only cover a limited set of possible inclination angles, this method is useful only for a few inclinations. Atakan et al. [7], [8] proposed a mode intent recognition to discriminate between standing, walking and sitting. Lawson et al. [9] provided stair ascending and descending within the same impedance framework. Even though these modes have been reported to be successful, user intent must be identified to switch between different modes. This requires some dramatic and/or unnatural leg movements and tends to introduce a delay on the walking activity. Additionally, misclassification might happen with these methods.

Electromyography (EMG) based methods have been implemented in the transfemoral prosthesis with the goal of achieving more natural actuation and motion transition [10]. EMG signals were mapped and classified to control each of the actuators. However, even with the successful implementation, EMG-based methods could suffer from misclassification issues. Copying kinematic data from one leg to another [11] could not compensate for the differences in terrain if the legs are in different terrains. Also, basic gait descriptors [12] may have problems to adapt to every slope presented. To avoid problems of parameter tuning and misclassification for intent recognition, we start from the human-inspired walking approach and move forward to an adaptive formulation.

The human-inspired walking approach has potentials to automatically generate stable and human-like walking gaits for transfemoral prosthesis. Ames et al. proposed to use human data in generating gait patterns originally for bipedal robots [13], [14]. Zhao et al. [3] adapted the human-inspired

*This work was supported by Texas Emerging Technology Fund 11062013.

¹Department of Mechanical Engineering, Texas A&M University, College Station, TX 77843, USA. vcparedesc@tamu.edu, ulim8819@tamu.edu, shawaneepatrick@tamu.edu, pilwonhur@tamu.edu

control method into the powered transfemoral prosthesis, where he showed stable and human-like prosthetic walking through experiments. The advantage of this framework is i) the avoidance of parameter tuning, and ii) the generation of a provably stable walking gait.

The human-inspired walking approach was also used for the generation of walking gaits to perform stair ascending [15]. The proposed method consisted in formulating human-inspired optimization with the stairs profile, which provides a provably stable walking gait. However, two drawbacks in this method must be mentioned: i) the human-inspired optimization needs to be executed offline, and ii) the *a priori* knowledge of the stairs profile (or any surface in general) might not be available in practical applications. In general, surface inclination is unknown in advance and can only be estimated upon contact with the surface. Furthermore, the human-inspired optimization cannot be solved online, which makes the framework impractical in reality.

The objective of this paper is the generation of upslope walking gaits for a continuous range of surface inclinations in real time in the transfemoral prosthesis AMPRO II developed by AMBER Lab [16]. To achieve this objective, we analyze human data and extract the basic strategies that humans use to generate seamless transition from flat ground walking to upslope walking. Cubic splines are generated through closed-form optimization that connect flat ground walking trajectories with upslope walking trajectories, creating a smooth transition that allows adaptability to diverse surface inclinations.

The idea behind the optimization is the possibility to generate a trajectory for different initial conditions that can be shaped by an appropriate selection of the cost function. Since we are dealing with human subjects we need a real time algorithm thus we formulate the optimization as a convex problem. We additionally introduce a low gain PD controller, used before impact with the ground, on the ankle and knee to have adaptability of the walking gait in various unknown terrains.

II. CONTROLLER CONSTRUCTION

The controller is constructed from the qualitative observation of ankle and knee trajectories from the human data. The idea is to blend the nominal trajectories for the flat ground with the trajectories for the upslope walking. A set of cubic splines is proposed for this purpose. Additionally, a low gain PD controller is employed to adaptively step on unknown surfaces upon contact in the later phase of gait cycle.

A. Human strategies for upslope walking

Human data from [17] are analyzed to capture ankle and knee trajectories during flat ground walking and upslope walking with slope inclinations of 5° , 8° and 10° (Fig. 1). Careful observation of the data can warrant a trend in the trajectories of ankle and knee as the slope increases (Fig. 1). As the slope increases, the initial and final phases of the trajectories increase in amplitude (Fig. 1). Please note that the trajectories converge to flat ground walking trajectories

between approximately 45% to 80% of the gait cycle. Similar trends can also be found in the human-inspired simulation for upslope walking [18], particularly in the increase on knee flexion during the beginning and the end of the gait cycle.

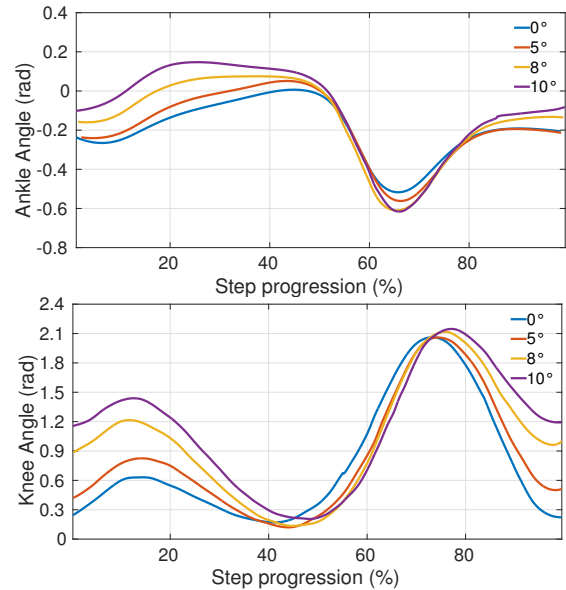


Fig. 1. Kinematic data showing the effect of the slope of an inclined surface. Data digitized from [17]

B. Prosthesis strategies

In order to qualitatively obtain similar strategies as human data exhibits, we apply two algorithms in different phases of the step progression. During the stance (i.e., early) phase of the prosthetic gait cycle, a region is selected from the beginning of the step to a point where the upslope and flat ground trajectories are converging (Fig. 1), from this point the algorithm blends the trajectories such that for any new initial condition a new trajectory is generated that converges to the flat ground walking trajectories. For swing (i.e., late) phase, a region is chosen in the last part of the step progression, from a point where the flat ground and upslope trajectories are starting to diverge to the final part of the step. In this region a low gain PD control is applied with the objective to allow the trajectories to adaptively be blended with the unknown surface. These regions are shown in Fig. 2. The low gain PD allows the prosthetic joints to accommodate unknown changes in surface.

The general action of the strategies expected on the prosthesis consists of i) active joint accommodation at the surface due to the low gain PD control, and ii) the qualitatively similar evolution of the joints trajectories during upslope walking with respect to the human strategies via splines generation. It is assumed that human is inherently robust and able to reject small perturbation due to trajectory blending.

The objective of this framework is to obtain the same qualitative behaviors for the ankle and knee. Note that these behaviors are expected to be replicated especially by the knee. Due to the imposition of flat foot walking, the ankle

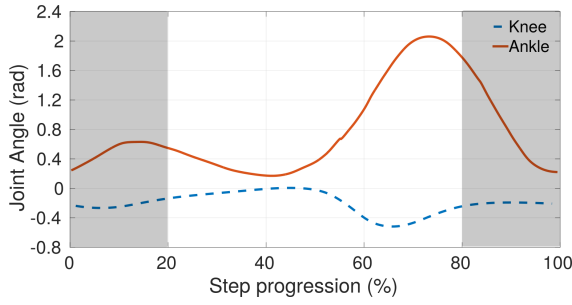


Fig. 2. Regions of action of the splines (white region) and the low gain PD control (shaded region).

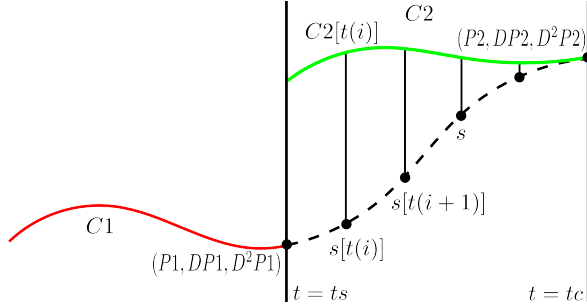


Fig. 3. Blending trajectory C1 to reach trajectory C2.

trajectories will evolve somewhat differently than the human ankle trajectories. A multi-contact algorithm would improve this. Online generation of a set of trajectories can overcome a range of different surfaces in real time. To our best knowledge, it is the first online optimization-based trajectory generation on prosthetic devices.

C. Cubic-splines based convex optimization

To generate the trajectories that blend the flat ground human trajectories in real time, we use a convex optimization formulation. Also, smoothness of the trajectory plays a key role in the performance since nonsmooth trajectories can cause large velocities or accelerations. However, smoothness condition entails more requirements in generating the trajectories. That is, the end point in the initial path C1 must be the starting point of the generated trajectory (see dashed line in Fig. 3) and the end point on the desired path C2, the nominal flat ground trajectory, must also be designed as an smooth connection guaranteeing smoothness in position, velocity and acceleration. The generated smooth trajectory S is expected to behave as shown in Fig. 3.

We are interested in formulating a set of N cubic splines rather than a single cubic spline since using a single cubic spline does not have enough freedom for better blending of two trajectories. The first conditions for smoothness are

addressed by imposing continuity in the extreme points.

$$S(t_s) = P1 \quad (1)$$

$$S(t_c) = P2 \quad (2)$$

$$\dot{S}(t_s) = dP1 \quad (3)$$

$$\dot{S}(t_c) = dP2 \quad (4)$$

$$\ddot{S}(t_s) = d^2P1 \quad (5)$$

$$\ddot{S}(t_c) = d^2P2 \quad (6)$$

where d represents a derivative operator. It is also necessary to ensure the smoothness along the generated path by imposing the previous constraints along all the waypoints $S(t(i))$. Let S_1 and S_2 be the two consecutive splines, connected at a waypoint $t(i)$. Then the conditions of smoothness can be written as:

$$S_1(T(i)) = S_2(T(i)) \quad (7)$$

$$\dot{S}_1(T(i)) = \dot{S}_2(T(i)) \quad (8)$$

$$\ddot{S}_1(T(i)) = \ddot{S}_2(T(i)) \quad (9)$$

To generate a trajectory that approaches the reference path C2, it is necessary to have a cost function based on the distance between the splines trajectory and C2. Fig. 3 shows the distance between each waypoint to the desired trajectory. These distances will be used to construct the cost function for the following least square formulation:

$$\min \sum_i ||S(T(i)) - C2(T(i))|| \quad (10)$$

$$st \quad (1) - (9) \quad (11)$$

Each cubic spline has the following form:

$$S_i = a_0^i + a_1^i(t - t_c) + a_2^i(t - t_c)^2 + a_3^i(t - t_c)^3 \quad (12)$$

Which, after derivations yields:

$$\dot{S}_i = a_1^i + 2a_2^i(t - t_c) + 3a_3^i(t - t_c)^2 \quad (13)$$

$$\ddot{S}_i = 2a_2^i + 6a_3^i(t - t_c) \quad (14)$$

Note that the splines S_i and S_{i+1} are continuous and smooth in terms of position, velocity and acceleration. For position, the following condition needs to be satisfied:

$$S_i(t_i) = a_0^i + a_1^i(\Delta t_i) + a_2^i(\Delta t_i)^2 + a_3^i(\Delta t_i)^3 \quad (15)$$

$$S_{i+1}(t_i) = a_0^{i+1} + a_1^{i+1}(\Delta t_i) + a_2^{i+1}(\Delta t_i)^2 + a_3^{i+1}(\Delta t_i)^3 \quad (16)$$

$$S_i(t_i) - S_{i+1}(t_i) = 0 \quad (17)$$

Repeating the same procedure for velocity, the following is obtained:

$$\dot{S}_i(t_i) = a_1^i + 2a_2^i(\Delta t_i) + 3a_3^i(\Delta t_i)^2 \quad (18)$$

$$\dot{S}_{i+1}(t_i) = a_1^{i+1} + 2a_2^{i+1}(\Delta t_i) + 3a_3^{i+1}(\Delta t_i)^2 \quad (19)$$

$$\dot{S}_i(t_i) - \dot{S}_{i+1}(t_i) = 0 \quad (20)$$

Finally, considering acceleration, the following conditions needs to be satisfied:

$$\ddot{S}_i(t_i) = 2a_2^i + 6a_3^i(\Delta t_i) \quad (21)$$

$$\ddot{S}_{i+1}(t_i) = 2a_2^{i+1} + 6a_3^{i+1}(\Delta t_i) \quad (22)$$

$$\ddot{S}_i(t_i) - \ddot{S}_{i+1}(t_i) = 0 \quad (23)$$

These constraints can be written in a matrix form. Considering λ a vector storing all the parameters of the splines, a segment $\lambda_{i,i+1}$ is constructed in the following way:

$$\lambda_{i,i+1} = [a_0^i \ a_1^i \ a_2^i \ a_3^i \ a_0^{i+1} \ a_1^{i+1} \ a_2^{i+1} \ a_3^{i+1}]^T \quad (24)$$

Then, the constraints can be written as follows:

$$\begin{bmatrix} 1 & \Delta t_i & \Delta t_i^2 & \Delta t_i^3 & -1 & -\Delta t_i & -\Delta t_i^2 & -\Delta t_i^3 \end{bmatrix} \lambda_{i,i+1} = 0 \quad (25)$$

$$\begin{bmatrix} 0 & 1 & 2\Delta t_i & 3\Delta t_i^2 & 0 & -1 & -2\Delta t_i & -3\Delta t_i^2 \end{bmatrix} \lambda_{i,i+1} = 0 \quad (26)$$

$$\begin{bmatrix} 0 & 0 & 2 & 6\Delta t_i & 0 & 0 & -2 & -6\Delta t_i \end{bmatrix} \lambda_{i,i+1} = 0 \quad (27)$$

With the boundary conditions for the initial point, we have:

$$\begin{bmatrix} 1 & \Delta t_0 & \Delta t_0^2 & \Delta t_0^3 & 0 & 0 & 0 & 0 \end{bmatrix} \lambda_{0,1} = P1 \quad (28)$$

$$\begin{bmatrix} 0 & 1 & 2\Delta t_0 & 3\Delta t_0^2 & 0 & 0 & 0 & 0 \end{bmatrix} \lambda_{0,1} = dP1 \quad (29)$$

$$\begin{bmatrix} 0 & 0 & 2 & 6\Delta t_0 & 0 & 0 & 0 & 0 \end{bmatrix} \lambda_{0,1} = d^2P1 \quad (30)$$

Analogous formulation for the other extreme point can be obtained for $P2, dP2, d^2P2$. All the constraints can be written in a single matrix, which is represented by the constraint matrix C .

$$C\lambda = D \quad (31)$$

where, D is the value that the equation must take in order to meet the constraint conditions, which can be $P1, dP1, d^2P1, P2, dP2, d^2P2$ or zero depending on the waypoint and the condition being enforced.

In order to express the cost function, it is possible to obtain the value of each spline at its respective waypoint using the following equation:

$$S_i(t_i) = \begin{bmatrix} 1 & \Delta t_i & \Delta t_i^2 & \Delta t_i^3 \end{bmatrix} \lambda_{i,i+1} = P_i \lambda_{i,i+1} \quad (32)$$

Then, all values at the waypoints are calculated in a vector using the following equation:

$$S = P\lambda \quad (33)$$

Finally, the minimization problem can be formulated as:

$$\min \|P\lambda - Y\| \text{ s.t. } C\lambda = D \quad (34)$$

where, Y is the desired set of points to which we want to converge to.

D. Analytical solution of optimization problem

It is possible to solve the optimization using an analytical form ready to be solved by most linear algebra C++ packages. Considering the problem expressed in the optimization, it is possible to rewrite the optimization problem as:

$$\min \|P\lambda - Y\| = \min \lambda^T P^T P \lambda - 2Y^T P \lambda + Y^T Y \quad (35)$$

$$\text{s.t. } C\lambda = D \quad (36)$$

The Lagrangian is:

$$L = \lambda^T P^T P \lambda - 2Y^T P \lambda + Y^T Y + v^T (C\lambda - D) \quad (37)$$

Then, the KKT conditions for optimality are:

$$2P^T P \lambda - 2P^T Y + C^T v = 0 \quad (38)$$

$$C\lambda = D \quad (39)$$

The matrixial form for the solution is written as:

$$\begin{pmatrix} 2P^T P & C^T \\ C & 0 \end{pmatrix} \begin{pmatrix} \lambda \\ v \end{pmatrix} = \begin{pmatrix} 2P^T Y \\ D \end{pmatrix} \quad (40)$$

$$\begin{pmatrix} \lambda \\ v \end{pmatrix} = \begin{pmatrix} 2P^T P & C^T \\ C & 0 \end{pmatrix}^{-1} \begin{pmatrix} 2P^T Y \\ D \end{pmatrix} \quad (41)$$

If C matrix is full-rank, then the matrix will be invertible. However, the matrix can become ill-posed. To avoid problem of ill-posedness, a regularization technique is used. The importance of the closed form formulation is i) the existence of a solution and ii) real time computation. Note that choosing a large number of splines may increase the optimization time, however, a small number of splines (4 splines) are used.

E. Splines simulation

The spline generation was tested in MATLAB. As shown in Fig. 4, the formulation of splines can generate a smooth trajectory that converges from any initial condition to the flat ground walking trajectories for both ankle and knee. The generated trajectories match the desired qualitative human walking trajectories.

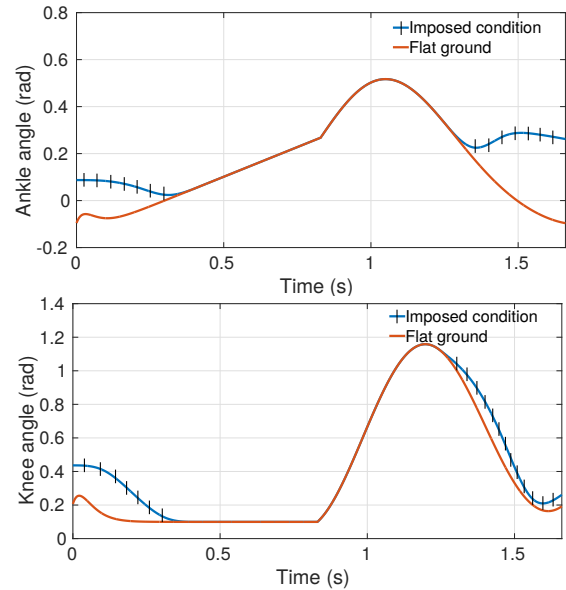


Fig. 4. Ankle and knee trajectories for flat ground walking and with imposed conditions for spline testing.

III. FLAT TERRAIN GAIT GENERATION

The goal of this section is to introduce the framework of generating a stable flat ground prosthetic walking gait that can be used as a reference to blend trajectories and generate upslope walking gaits. Firstly, a IMU based motion capture system is introduced to record healthy human data, which will be used as a reference point for human-like prosthetic gait design. In the context of human-inspired optimization

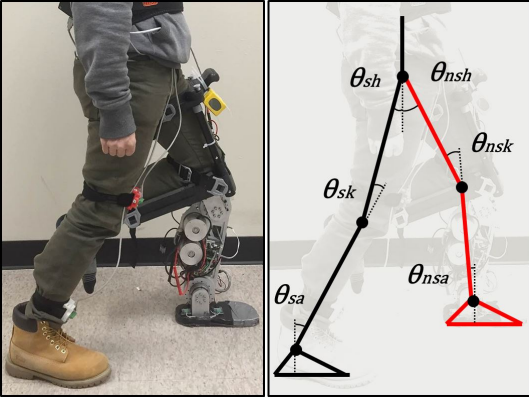


Fig. 5. Robotic model inspired on the human subject.

[13], a bipedal robot system is considered for the human-prosthesis model. Based on this model, the human-inspired optimization problem is implemented to generate a stable prosthetic gait that can also be implemented on the device directly.

A. Motion capture

During the data recording procedure, an External Kalman Filter (EKF) is utilized to estimate the ankle and knee trajectories, which will be used as a reference for prosthetic gait design. In order to generate a stable walking gait for a prosthetic device using the human-inspired approach, we follow the procedure followed in AMPRO I [3]. An IMU based inertial motion capture system is used to record the joint trajectories of a healthy subject with similar anthropomorphic dimensions with respect to the prosthesis user (that could be an amputee). The IMU data is processed using an External Kalman Filter (EKF) to determine the estimated trajectories of the ankle and knee needed for the human-inspired optimization.

B. Prosthetic model construction

1) *Robotic Model*: We model the human-prosthetic walking as a 7-link (one torso, two thighs, two calves and two feet) bipedal robotic system which shares similar anthropomorphic values as the prosthesis user. The coordinates are defined as $\theta = (\theta_{sa}, \theta_{sk}, \theta_{sh}, \theta_{nsh}, \theta_{nsk}, \theta_{nsa})^T \in Q_R$ as in Fig. 5. Using the Euler-Lagrange, the dynamics can be expressed:

$$D(\theta)\ddot{\theta} + C(\theta, \dot{\theta})\dot{\theta} + G(\theta) = Bu \quad (42)$$

where, $D(\theta) \in \mathbb{R}^{6 \times 6}$ is the inertial matrix, $C(\theta, \dot{\theta})$ is the coriolis matrix, $G(\theta)$ is the gravity vector and $B = I_6$ is the torque map. By defining the state vector $x = (\theta, \dot{\theta})^T$ it is possible to formulate (42) as an affine control system with the following equations:

$$\dot{x} = f(x) + g(x)u \quad (43)$$

Considering the existence of impacts when the swing leg hits the ground, the system is naturally modeled as a hybrid system. Perfect plastic impact model (i.e., there is no rebound, slipping or deformation during the impact [19]) is adopted

to model the impact dynamics in this work. A detailed description of hybrid systems applied to bipedal robots can be referred to [13], [20], [21].

2) *Human-Inspired Outputs*: To represent human locomotion from a control perspective, a set of outputs—joint angles or functions of joint angles—is utilized to characterize human walking kinematically. Therefore, the goal of achieving human-like walking becomes to drive the actual robot outputs $y^a(\theta)$ to the desired human outputs $y^d(t, \alpha)$, which is represented by a set of canonical walking functions (CWF) with parameter α [13]. Note that, with the analysis of human locomotion data, it is found that the forward hip position $\rho(\theta)$ progresses linearly during a step cycle [14]. In light of this observation, we use $\rho(\theta)$ as a phase variable to remove time dependency of the tracking functions, making the tracking system autonomous. In particular, we define the following parameterized virtual constraints as:

$$y(\theta, \dot{\theta}, \alpha) = \begin{bmatrix} y_1(\theta, \dot{\theta}, \alpha) \\ y_2(\theta, \alpha) \end{bmatrix} = \begin{bmatrix} y_1^a(\theta, \dot{\theta}) - v_{hip} \\ y_2^a(\theta) - y_2^d(\rho(\theta), \alpha) \end{bmatrix} \quad (44)$$

where, $y_1(\theta, \dot{\theta}, \alpha)$ is the relative degree one output corresponding to the difference between the actual hip velocity $y_1^a(\theta, \dot{\theta})$ and the desired hip velocity v_{hip} . $y_2(\theta, \alpha)$ are the relative degree two virtual constraints which are the difference between the actual $y_2^a(\theta)$ outputs and the desired $y_2^d(\rho(\theta), \alpha)$ outputs. Note that, in order to achieve stable tracking for the hybrid system, the controller parameters α will be obtained from a human-inspired optimization problem that will be discussed in the following section.

Partial Hybrid Zero Dynamics. A regular feedback linearization controller that yields $y(\theta, \dot{\theta}, \alpha) \rightarrow 0$ for continuous dynamics can not guarantee stable bipedal walking considering the embedded hybrid property (i.e., impacts) of such systems. This motivates the introduction of the partial hybrid zero dynamics (PHZD) constraints aiming to yield a parameter set α that ensures the tracking of relative degree two outputs remain invariant through impacts. In particular, we define the PHZD surface as:

$$PZ_\alpha = \{(\theta, \dot{\theta}) \in TQ_R : y_2(\theta, \alpha) = 0, L_f y_2(\theta, \alpha) = 0\} \quad (45)$$

This surface is impact invariant if the following PHZD constraint holds:

$$\Delta_R(S_R \cap PZ_\alpha) \subset PZ_\alpha \quad (46)$$

where Δ_R and S_R are the reset map and the switching surface corresponding to the model. A detailed mathematical construction of these two terms can be found in [13], [14].

3) *Human-Inspired Optimization*: A human-inspired optimization problem is implemented here to generate a human-like stable gait for flat-ground walking. The human locomotion data collected by the IMU system is used as the reference trajectory for the optimization problem. In particular, we define the objective cost function as the weighted square sum of the differences between the actual human data and the desired tracking function, which guarantees the generated gait is as close to the healthy human trajectory as possible.

Additionally, the PHZD constraint (46) along with several physical constraints (such as torque, position and velocity limits imposed by the device) are considered explicitly for this optimization problem. Therefore, the human-inspired optimization can be formulated as:

$$\begin{aligned} \alpha &= \underset{\alpha \in \mathbb{R}^{26}}{\operatorname{argmin}} \quad \operatorname{Cost}_{HD}(\alpha) & (\text{HIO}) \\ & \text{s.t.} \quad (\text{PHZD}) \\ & \quad (\text{Physical Limitations}) \end{aligned}$$

The end result of this optimization is a mathematically stable gait which can also be implemented onto the physical device directly. The corresponding ankle and knee trajectories of the generated gait are shown in Fig. 4.

C. Outputs for upslope walking using splines

In order to introduce the generated splines into the CWF, it is important to consider the designed convergence time $t_c = \rho^*$. For each $\rho(\theta)$ less than ρ^* the splines trajectory will be used instead of the nominal CWF. The values of the splines can be calculated as:

$$S(\rho(\theta)) = [1 \quad \rho(\theta) \quad \rho(\theta)^2 \quad \rho(\theta)^3] \lambda_{i(\rho(\theta))} \quad (47)$$

where, $\lambda_{i(\rho(\theta))}$ is the set of spline parameters corresponding to $\rho(\theta)$. The relative degree two output will depend on $\rho(\theta)$ since it can be based on the spline trajectory or the CWF and is therefore defined as:

$$y_2(\theta, \alpha) = \begin{cases} y_2^d(\theta) - S(\rho(\theta)), & \text{if } \rho(\theta) \leq \rho^* \\ y_2^d(\theta) - y_2^d(\rho(\theta), \alpha), & \text{if } \rho(\theta) > \rho^* \end{cases} \quad (48)$$

Once the outputs are defined, a feedback controller can be used to drive the outputs to zero. Note that the splines may live outside the PHZD surface, this violation of the originally designed PHZD surface (for flat ground) is assumed to be handled by the human subject for the period of time where $\rho(\theta) < \rho^*$.

D. Control Implementation

With the desired joint values for position and velocity being calculated from the PHZD reconstruction [22], a PD controller is utilized to drive the prosthetic joints, which can be given by:

$$\tau_i = k_p^i(\theta_d^i - \theta_a^i) + k_d^i(\dot{\theta}_d^i - \dot{\theta}_a^i), i \in \{\text{ankle, knee}\} \quad (49)$$

During the last portion of prosthetic swing phase, (Fig. 2) the PD gains are decreased to create an effect of a low-impedance behavior, which allows the unknown terrain to determine the final joint position of the prosthesis.

IV. EXPERIMENT IMPLEMENTATION

A. AMPRO II

The proposed framework was implemented on a powered transfemoral prosthesis AMPRO II, which is the second version of the AMPRO prosthesis series that are custom designed by AMBER Lab [16] led by Dr. Aaron Ames at Texas A&M University (now at Georgia Tech) and

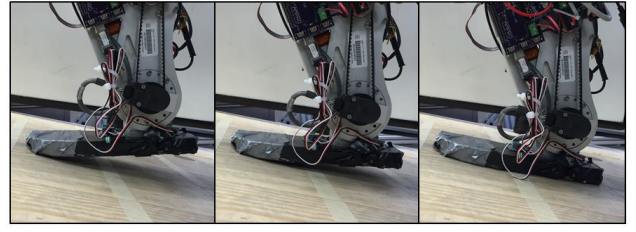


Fig. 6. Low gain PD representation of the action on a sloped surface.

maintained and operated by HUR Group at Texas A&M University for controller design. Compared to AMPRO I [3], the main improvements of AMPRO II are three folds: a) the weight is reduced to 5kg, which is more than 3kg weight reduction; b) the height is reduced by 71mm and the width is reduced by 36mm. The smaller size will allow a wider height range of subjects to be able to use this device; c) the motors and electronics are placed higher up on the calf resulting a higher center of mass position, which yields a much smaller inertial for the device. Additionally, two FlexiForce force sensors are mounted on the heel and toe for contact detection and leg switch. The main code structure including the online gait generation code is running on a low-power single core micro computer BeagleBone Black at 200Hz. Details of the design diagram can be seen in Fig. 7.

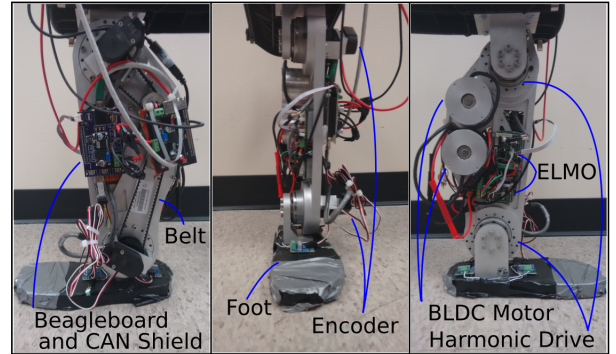


Fig. 7. AMPRO II prosthetic device developed by the AMBER Lab led by Dr. Ames. Each component is shown in one of the three views of the prosthesis.

B. Human-Robotic Interfacing

As discussed in Section III, the forward hip position $\rho(\theta)$ is utilized as the phase variable to parameterize one step. In this manner, the desired trajectories for the prosthetic joints can be determined based on the current hip position which is measured based on the stance leg [3]. During the prosthetic stance phase, the $\rho(\theta)$ can be calculated utilizing the encoder readings. In order to provide a sensor feedback during human stance phase, i.e., to calculate the phase variable during the human stance phase, two IMUs are mounted on the shin and thigh of the human leg. The end result is that the prosthetic leg could sync with the human leg movement based on the calculation of hip position utilizing the IMUs readings.

C. Experimental Results

During the experiment, the prosthesis user was requested to walk indoors from flat ground to upslope as shown in Fig. 10. The walking surface of the testing consists a 13ft flat walkway leading directly to a 7ft 13° slope surface. The resulting ankle and knee trajectories of both flat ground and upslope walking are shown in a comparative way in Fig. 8, from which we can see that the strategies observed in human walkers are replicated qualitatively in the prosthesis knee joint. The differences in ankle trajectories with respect to normal human walking are originated because of the imposition of flat foot walking, instead of a more natural multi-contact walking algorithm (heel strike, toe push) [23], [24], [25]. Note that during flat ground walking, the framework yielded a stable prosthetic walking for the user as suggested by Fig. 10. Furthermore, from this figure we can see that the transition from flat ground to upslope is done in real time without any delay or switching procedure.

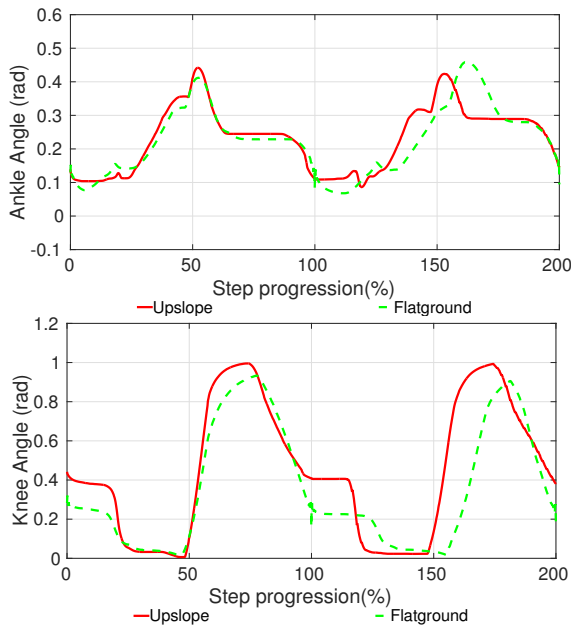


Fig. 8. Ankle and Knee (from top to bottom) trajectories for flat ground and upslope walking

The tracking results of both the ankle and knee trajectories during two walking steps are shown in Fig. 9. In 9, the duration of action of the low gain PD and the spline blending are presented by red and blue regions, respectively. It can be observed that the action of the low gain PD control allows actual joints position to diverge from its desired values which, therefore, give the user ability for terrain adaptation (see red region). Also, during the action of the splines, the actual values of the joint positions are taken as an initial point to generate a trajectory via the splines formulation that converges to the nominal flat ground trajectories and shows qualitatively similar behavior that the upslope human trajectories (see blue region). Also, an outdoor experiment was realized with AMPRO II, resulting in stable walking for flat ground and upslope surfaces as shown in in Fig. 11.

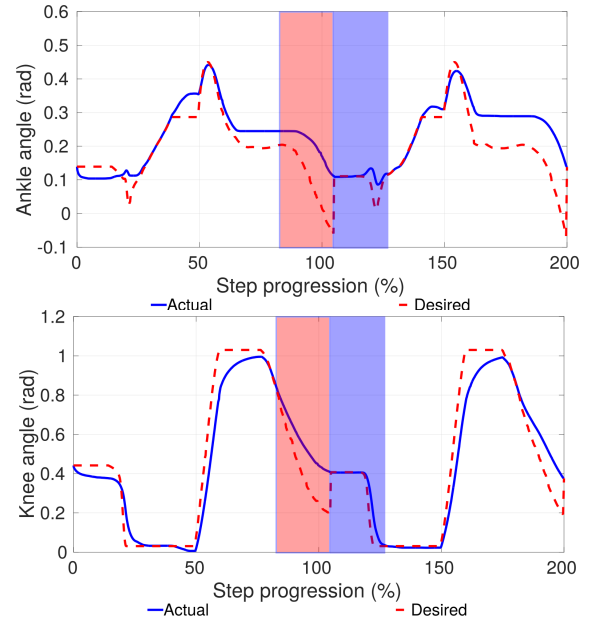


Fig. 9. Ankle and Knee trajectories for upslope walking, the red region indicates the area of action of the low PD gain, and the blue are the splines generation

V. CONCLUSIONS

The proposed framework for upslope walking allows the prosthesis user to traverse unknown sloped surfaces. Given any unknown surface inclination, the proposed algorithm generates a specific set of trajectories for every condition that is imposed by the surface. In particular, this framework did not require any tuning processes for the determination of controller gains during upslope walking. Additionally, only one-time human-inspired optimization for the flat ground (for reference trajectory) was needed to be conducted offline. Due to these benefits, this framework can be utilized in other devices with real time solutions. The splines generated satisfy smoothness conditions that are key for its implementation, a small number of splines (4 splines) were chosen because a large number of them would unnecessarily increase the computation time. The splines are defined by the time designed to converge (t_c), since the initial time is assumed at the beginning of the step ($t_s = 0$).

Due to the flat-foot walking assumption, the prosthetic trajectories are different with the healthy human trajectories, specially in the ankle. This situation can be improved by implementing a more natural multi-contact gait [23] that considers heel-strike and toe-push.

REFERENCES

- [1] Owings Maria F. and Kozak Lola Jean. Ambulatory and inpatient procedures in the united states, 1996. *National Center for Health Statistics.*, Vital Health(Stat 13(139)), 1998.
- [2] Douglas G. Smith. The transfemoral amputation level, part 1. URL: "http://www.amputee-coalition.org/resources/transfemoral-amputation-part-1/", Accessed: 03/01/2016.
- [3] Huihua Zhao, Jake Reher, Jonathan Horn, Victor Paredes, and Aaron D. Ames. Realization of nonlinear real-time optimization based controllers on self-contained transfemoral prosthesis. In ACM,



Fig. 10. Prosthesis user walking from flat ground to upslope (<https://youtu.be/Qze2SGNOyUI>).



Fig. 11. Prosthesis user walking upslope in outdoors environment (<https://youtu.be/Qze2SGNOyUI>).

editor, *Proceedings of the ACM/IEEE Sixth International Conference on Cyber-Physical Systems.*, 2015.

- [4] Frank Sup, Amit Bohara, and Michael Goldfarb. Design and control of a powered transfemoral prosthesis. *The International Journal of Robotics research.*, 27(2):263–273, 2008.
- [5] Robert D Gregg and Jonathon W Sensinger. Towards biomimetic virtual constraint control of a powered prosthetic leg. *Control Systems Technology, IEEE Transactions on*, 22(1):246–254, 2014.
- [6] Frank Sup, Huseyin Atakan Varol, and Michael Goldfarb. Upslope walking with a powered knee and ankle prosthesis: initial results with an amputee subject. *Neural Systems and Rehabilitation Engineering, IEEE Transactions on.*, 19(1):71–78, 2011.
- [7] Huseyin Atakan Varol, Frank Sup, and Michael Goldfarb. Real-time gait mode intent recognition of a powered knee and ankle prosthesis for standing and walking. In *Biomedical Robotics and Biomechanics, 2008. BioRob 2008. 2nd IEEE RAS & EMBS International Conference on*, pages 66–72. IEEE, 2008.
- [8] Huseyin Atakan Varol, Frank Sup, and Michael Goldfarb. Multiclass real-time intent recognition of a powered lower limb prosthesis. *Biomedical Engineering, IEEE Transactions on*, 57(3):542–551, 2010.
- [9] Brian E Lawson, Huseyin Atakan Varol, Amanda Huff, Erdem Erdemir, and Michael Goldfarb. Control of stair ascent and descent with a powered transfemoral prosthesis. *Neural Systems and Rehabilitation Engineering, IEEE Transactions on*, 21(3):466–473, 2013.
- [10] Levi J Hargrove, Ann M Simon, Aaron J Young, Robert D Lipschutz, Suzanne B Finucane, Douglas G Smith, and Todd A Kuiken. Robotic leg control with emg decoding in an amputee with nerve transfers. *New England Journal of Medicine*, 369(13):1237–1242, 2013.
- [11] Heike Vallery, Edwin HF van Asseldonk, Martin Buss, and Herman van der Kooij. Reference trajectory generation for rehabilitation robots: complementary limb motion estimation. *IEEE transactions on neural systems and rehabilitation engineering*, 17(1):23–30, 2009.
- [12] Letian Wang, Edwin HF van Asseldonk, and Herman van der Kooij. Model predictive control-based gait pattern generation for wearable exoskeletons. In *2011 IEEE International Conference on Rehabilitation Robotics*, pages 1–6. IEEE, 2011.
- [13] Aaron D. Ames. First steps toward automatically generating bipedal walking from human data. *Robot Motion and Control 2011*, Springer London:89–116, 2012.
- [14] Aaron D. Ames. Human-inspired control of bipedal walking robots. *IEEE Transactions on Automatic Control.*, 59(5), 2014.
- [15] Huihua Zhao, Jake Reher, Jonathan Horn, Victor Paredes, and Aaron D. Ames. Realization of stair ascent and motion transitions on prostheses utilizing optimization-based control and intent recognition. In IEEE, editor, *Rehabilitation Robotics (ICORR), 2015 IEEE International Conference on.*, 2015.
- [16] Amber lab. www.bipedalrobotics.com. Accessed: 2016-08-01.
- [17] Andrew Stuart McIntosh, Karen T. Beatty, Leanne N. Dwan, and Deborah R. Vickers. Gait dynamics on an inclined walkway. *Journal of Biomechanics.*, 39(13):2491–2502, 2006.
- [18] Huihua Zhao and Aaron D Ames. Quadratic program based control of fully-actuated transfemoral prosthesis for flat-ground and up-slope locomotion. In *American Control Conference (ACC), 2014*, pages 4101–4107. IEEE, 2014.
- [19] E. R Westervelt, J. W. Grizzle, C Chevallereau, J Choi, and B. Morris. *Feedback control of dynamic bipedal robot locomotion*. CRC press, 2007.
- [20] E.R Westervelt, J.W Grizzle, and Koditscheck. D.E. Hybrid zero dynamics of planar biped walkers. *IEEE Transactions on Automatic Control*, 48(1):42–56, 2003.
- [21] Benjamin Morris and Jessy W Grizzle. Hybrid invariant manifolds in systems with impulse effects with application to periodic locomotion in bipedal robots. *Automatic Control, IEEE Transactions on*, 54(8):1751–1764, 2009.
- [22] Wen-Loong Ma, Huihua Zhao, Shishir Kolathaya, and Aaron D Ames. Human-inspired walking via unified pd and impedance control. In *Robotics and Automation (ICRA), 2014 IEEE International Conference on*, pages 5088–5094. IEEE, 2014.
- [23] Huihua Zhao, Jonathan Horn, Jacob Reher, Victor Paredes, and Aaron D Ames. Multi-contact locomotion on transfemoral prostheses via hybrid system models and optimization-based control.
- [24] Huihua Zhao, Wen-Loong Ma, Michael B. Zeagler, and Aaron. D. Ames. Human-inspired multi-contact locomotion with amber2. *ACM/IEEE 5th International Conference on Cyber-Physical Systems (with CPS Week 2014)*, IEEE Computer Society, 2014.
- [25] Jordan Lack, Matthew J Powell, and Aaron D Ames. Planar multi-contact bipedal walking using hybrid zero dynamics. In *Robotics and Automation (ICRA), 2014 IEEE International Conference on*, pages 2582–2588. IEEE, 2014.